



Beam merging assisted by a bent crystal

W. Scandale^{1,2,a}, F. Cerutti³, L. S. Esposito³, S. Gilardoni³, R. Losito³, G. I. Smirnov³, A. Giribono⁴, M. Bauce², F. Collamati², P. Valente², A. Variola^{2,b}, F. Galluccio⁵, G. Hall¹, M. Pesaresi¹, K. Uchida¹, R. Rossi^{1,3}

¹ Blakett Laboratory, Imperial College, London SW7 2AZ, UK

² INFN, Sezione di Roma, Piazzale Aldo Moro 2, 00185 Rome, Italy

³ The European Organization for Nuclear Research (CERN), CH-1211 Geneva 23, Switzerland

⁴ INFN, Laboratori Nazionali di Frascati, Via Fermi, 40, 00044 Frascati, Roma, Italy

⁵ INFN, Sezione di Napoli, Complesso Universitario di Monte Sant'Angelo, Via Cintia, 80126 Napoli, Italy

Received: 13 July 2023 / Accepted: 16 October 2023

© The Author(s) 2023

Abstract Bunch merging is a well-established technique to increase the intensity of synchrotrons and the luminosity of circular colliders. We suggest to exploit a combination of channeling, volume reflection and amorphous interactions in a bent crystal for beam merging in a transfer line. Two beams converging into the bent crystal along special directions should emerge in almost parallel directions. A merging scenario is discussed, and data collected by the UA9 Collaboration are reprocessed to prove its feasibility. Comparison with magnetic stacking, which is a similar process, is presented.

1 Introduction

Charged particle interactions with crystals depend on the incident angle θ of particle trajectories with respect to the crystalline planes because of anisotropy of the medium [1]. At small values of θ , particles may be captured in channeling states (CH) into the electrostatic potential of the regularly distributed nuclei, giving rise to reduced probability of multiple Coulomb scattering (MCS), inelastic nuclear interactions (INI) and ionization loss. Particle confinement requires that $\theta \leq \theta_c$, where $\theta_c = \sqrt{2U_{\max}/pv}$ is the channeling critical angle, U_{\max} is the potential well between two crystalline planes (~ 20 eV for Si (110) planes), and p and v are the particle momentum and velocity, respectively [1]. In a bent crystal, particles may be channeled if the bending radius R is larger than the critical value $R_c = E/eE_m$, where E is the particle energy and E_m is the maximum strength of the atomic electric field averaged along the planes ($E_m \approx 6$ GV/cm for Si (110) planes) [2]. As R decreases, the inter-planar potential well becomes increasingly asymmetric and ineffective, and the critical angle is reduced [3, 4]. Crystals bent by the angle θ_b can deflect incoming particles, through channeling (CH) or volume reflection (VR). Deflection angles are $\theta_{\text{CH}} = \theta_b$ and $\theta_{\text{VR}} \simeq 1.3 \times \theta_c$, respectively [5]. Particles in channeling states at the crystal entry face may be dechanneled (DCH), i.e., jump out of the potential well, because of the MCS with the nuclei and the electrons of the crystal atoms. DCH particles are bent by an angle $\theta < \theta_b$ proportional to the path length in CH states. Particles entering the crystal with an incident angle $\theta \gg \theta_b$ see the crystal as an isotropic medium and follow "amorphous" trajectories (AM) only perturbed by MCS [4]. Deflection efficiency, i.e., the ratio of deflected by incident particle flux, differs for positive and negative charges [4].

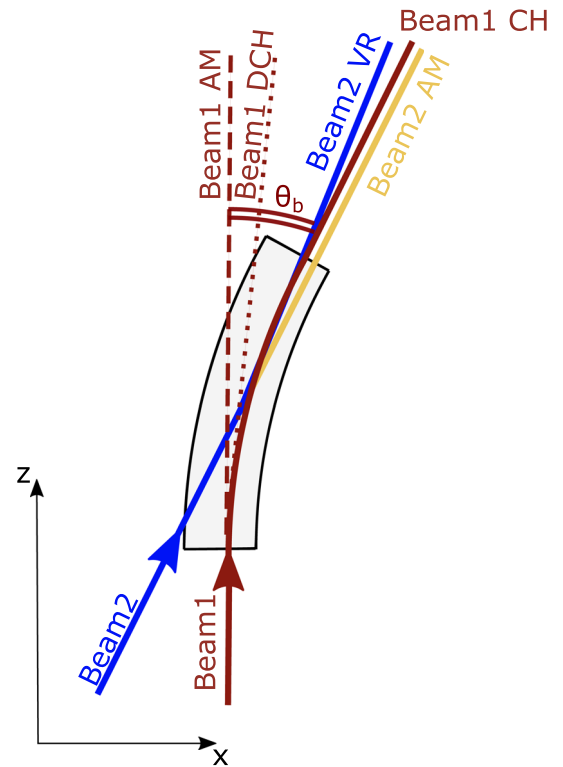
A number of beam manipulations assisted by bent crystals [2] is routinely exploited for operational tasks in particle accelerators and beam lines. Simultaneous kaon beams, produced in the North Area of SPS using a bent crystal as a splitter, were exploited during several years by the NA48 experiment at CERN [6, 7]. Crystal assisted proton extraction is routinely performed in several sections of the U70 synchrotron at IHEP in Protvino [8, 9]. Loss reduction at the SPS extraction relies on a bent crystal acting as a smart scatterer in front of the electrostatic septum wires [10]. Halo collimation based on crystals is the operational base-line at the LHC during ion collision runs and low-intensity proton operation (e.g., for TOTEM dedicated runs) [11].

In this article, we propose a method for beam merging assisted by a bent crystal. Two beams interacting with the crystal along appropriate directions can be deflected along almost parallel paths. For the preliminary validation of such process, a high statistics data set acquired earlier with the UA9 setup [12] is exploited and reprocessed. Emittance after merging by the bent crystal is computed and compared to that resulting from transverse beam stacking [13].

^a e-mail: walter.scandale@cern.ch (corresponding author)

^b e-mail: alessandro.variola@lnf.infn.it (corresponding author)

Fig. 1 Two-beam merging scheme. Beam1 (red line) enters the crystal in the CH direction; a fraction, captured in CH states, is bent by θ_b (double stroke red line), a fraction is dechanneled (dotted red line) and bent by $\theta < \theta_b$ and a fraction travels along AM paths (dashed red line). Beam2 (blue line) enters the crystal from the side performing AM (yellow line) or VR interactions (blue line)



2 Schematic description of beam merging assisted by a bent crystal

The conceptual description of a basic two-beam merging scenario assisted by a bent crystal is shown in Fig. 1. Beam1 (red line) and Beam2 (blue line) converge at the crystal with an angle θ_b . Beam1 is in optimal orientation for CH. Beam2 enters the crystal with a different incident angle, headed toward the edge of VR and AM orientations. At the crystal exit, the CH fraction of Beam1 is deflected by θ_b , the dechanneled fraction emerges in the angular range $0 < \theta < \theta_b$ (dotted red line) while the AM fraction continues straight, experiencing MCS (dashed red line). Particles in Beam2 are either deflected in VR or only undergo MCS along AM paths. The CH fraction of Beam1 (red line) and the VR (blue line) and AM (yellow line) fractions of Beam2 exit the crystal in almost parallel directions. The dechanneling process that reduces CH fraction of Beam1 and angular spread of concurrent VR and AM interactions in Beam2, brings inefficiency to the process of beam mixing. To increase the merging efficiency and maximize the merged beam density, the incident beam emittances should be well matched to the crystal features. In particular, the size of the incident beams should not exceed the crystal width, while the angular spread should be contained in the $\pm\theta_c$ range, to minimize the number of particles that cannot contribute to the two-beam merging. The process optimization will be thoroughly discussed in a separate paper.

An alternative procedure, exploiting VR and AM interactions only, will be discussed in a separate paper. It is expected to be rather efficient in recombining negatively charged beam particles because of the large VR deflection efficiency [14]. However, its practical implementation may be limited by small incident angles and reduced separation of Beam1 and Beam2 trajectories.

3 Using a UA9 crystal data-set for a merging scenario

A thought experiment is proposed to investigate the feasibility of the merging process. The data collected in a high-statistics run, in which a UA9 bent crystal was irradiated, are reworked to extract two subsets of trajectories representing Beam1 and Beam2. When superimposing the two beam trajectories, a realistic beam merging materializes, representing well the one discussed in Sect. 2.

3.1 The UA9 crystal data-set

The test crystal conceived to assist collimation in LHC was also exploited for accurate measurements of the INI cross-section [12]. It is made of a rectangular silicon strip, cut along the (110) planes, bent in a c-shaped titanium holder that imparts a vertical primary curvature and an almost circular anticlastic curvature in the horizontal mid-plane. Its features are summarized in Table 1, where X is the horizontal coordinate, Y the vertical one, and Z the longitudinal axis along which the incoming beam travels. The measured

Table 1 Parameters of the crystal ACP80: physical dimensions (L_X, L_Y, L_Z), bending angle (θ_b), bending radius (R), residual torsion around the Y-axis (T_Y)

Crystal	L_X mm	L_Y mm	L_Z mm	θ_b μrad	R m	T_Y $\mu\text{rad mm}^{-1}$
ACP80	3.00 ± 0.02	50.00 ± 0.1	4.00 ± 0.02	60.9 ± 0.5	65.7 ± 1	0.28 ± 0.25

Fig. 2 Track outgoing angle as a function of the incident angle on the crystal. The shaded vertical bands highlight the ranges of incident angles used to select particle distributions of Beam1 (red) and Beam2 (blue) that should contribute to beam merging

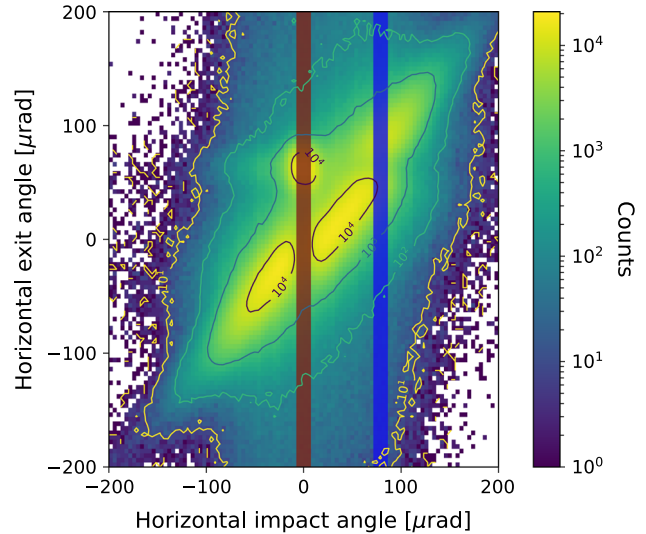


Table 2 Performance of the crystal ACP80: ϵ_{CH} is the CH efficiency, ϵ_{VR} is the VR efficiency, and $(\sigma_{\theta_{out}}/\sigma_{\theta_{in}})_{AM}$ and $(\sigma_{\theta_{out}}/\sigma_{\theta_{in}})_{VR}$ are the increase in the beam divergence in AM and VR orientations, respectively

Crystal	ϵ_{CH} $\theta \leq \theta_c$	ϵ_{CH} $\theta \leq \theta_c/2$	ϵ_{VR} $2\theta_c \leq \theta \leq 3\theta_c$	$(\sigma_{\theta_{out}}/\sigma_{\theta_{in}})_{AM}$ $-5\theta_c \leq \theta \leq -4\theta_c$	$(\sigma_{\theta_{out}}/\sigma_{\theta_{in}})_{VR}$ $2\theta_c \leq \theta \leq 3\theta_c$
ACP80	$(52.1 \pm 0.4)\%$	$(65.6 \pm 0.9)\%$	$(83.9 \pm 0.6)\%$	3.26 ± 0.05	3.39 ± 0.07

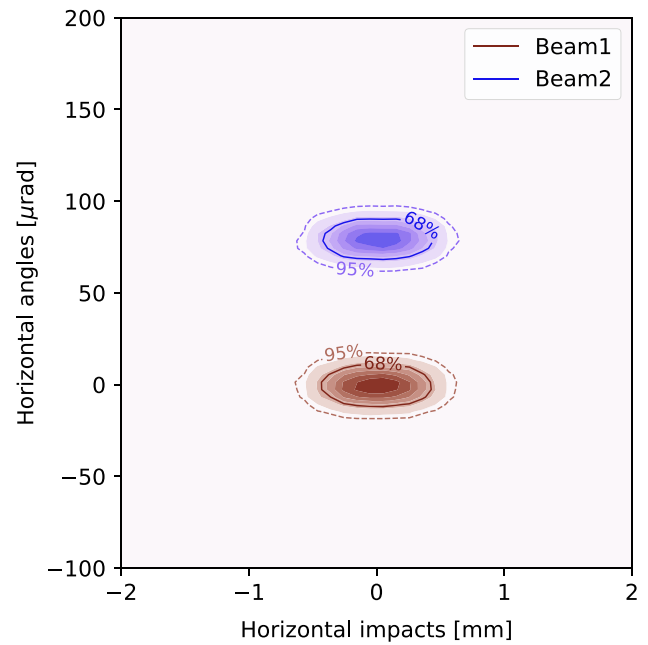
values of the radius of curvature R and of the residual torsion around the Y-axis (T_Y) are also reported. The name ACP80 was originally assigned to the test crystal by the crystal builder. Data were collected in the CERN North Area by irradiating the crystal ACP80 with a 180 GeV secondary hadron beam, composed of 70% protons and 30% pions with positive charge. At this energy, the critical angle and radius are $\theta_c \simeq 16 \mu\text{rad}$ and $R_c = 0.67 \text{ m}$, respectively.

The two-arm UA9 telescope was used to record the trajectories of the beam particles interacting with the crystal. The angular resolution was $12.3 \mu\text{rad}$, determined by the MCS in the silicon strip stations and the residual air [15–17]. In a typical run, trajectories were recorded while varying the crystal horizontal angle θ with respect to the beam reference axis. The optimal orientation for channeling θ_{CH} was identified. The angular range $-100 \mu\text{rad}$ to $150 \mu\text{rad}$ that encloses θ_{CH} was explored in steps of about $10 \mu\text{rad}$. The tracks were reconstructed in a reference frame, which was reoriented to be centered on the measured value of θ_{CH} . The realigned tracks of all runs were written to a single merged file and used for data analysis. Figure 2 displays the outgoing angles θ_{out} as a function of the incident angles θ_{in} . Each vertical line of the plot gives the data collected at a fixed orientation of the crystal. The color code represents the particle flux measured in a given outgoing direction. The colored vertical bands span the regions where the particles of Beam1 (brown band) and Beam2 (blue band) are selected (see next subsection). The CH and VR deflection efficiencies, ϵ_{CH} and ϵ_{VR} , respectively, and the beam divergence increase induced by MCS in AM and VR orientations, $(\sigma_{\theta_{out}}/\sigma_{\theta_{in}})_{AM}$ and $(\sigma_{\theta_{out}}/\sigma_{\theta_{in}})_{VR}$, respectively, evaluated by applying the UA9 procedures [18], are reported in Table 2. The latter results depend on the selected angular range of the incident beam particles, as discussed in [4, 18]. In Table 2, efficiency and beam divergence evaluations are shown for different angular ranges.

3.2 Incident beams and results of merging process

The particle trajectories of Beam1 and Beam2 are extracted from the population in the brown and blue bands of Fig. 2, respectively. This implies that the two beam axes converge toward the crystal at an angle $\theta_{B1-B2} = 80 \mu\text{rad} \simeq \theta_b + \theta_{VR}$. For an efficient beam merging assisted by a bent crystal, incident beam emittances should be matched in width and angular spread to the crystal features.

Fig. 3 Density distribution of Beam1 and Beam2 at the crystal entry face in the phase space (x , x'). Contour lines highlight the 68% and the 95% of each beam population



To implement such a feature, we define Beam1 and Beam2 with 2D Gaussian distribution in the (x , x') phase space at the crystal entrance. The data for each selection of the recorded trajectories are redistributed according to a normal Probability Density Function (PDF). The distribution of incident points on the crystal entry face is Gaussian with mean value $\langle x \rangle = 0$ and standard deviation $\sigma_x = 0.2$ mm, in both beams. The distribution of the incident angle is also Gaussian with standard deviation $\sigma_{x'} = 8$ μrad in both beams while the mean values differ for Beam1 and Beam2, the former being $\langle x' \rangle = 0$ and the latter $\langle x' \rangle = 80$ μrad , to implement the desired crossing angle. The entire set of particles of each beam crosses the crystal face because σ_x has been chosen to be sufficiently small ($L_X = 15 \times \sigma_x$). The dechanneling process in Beam1 is not predominant while the VR and AM interaction rates in Beam2 are comparable due to the choice of incident angle [4] and because $\sigma_{x'} \simeq \theta_c/2$. The beam density distributions at the crystal entry face are shown in Fig. 3. During crystal traversal, a fraction of Beam1 particles is captured in CH, while Beam2 particles experience either VR or AM interactions depending on small variations of their path along the crystal. The distribution of the outgoing trajectories at the exit face of the crystal, shown in Fig. 4 by light-blue and light-brown colored area, represents the distribution of the merged beam. Black continuous lines represent the area that contains 68% of the outgoing particles, while the green continuous line is the elliptical interpolation of such an area. Black and green dashed lines identify the area and its elliptical interpolation that contains 95% of the outgoing particles. Projections on the axes of the phase space, also shown in Fig. 4, illustrate the separate contributions of CH and VR events to the merging process.

4 Merging performance

To provide performance evaluation of the merging scenario assisted by the crystal ACP80, we compare it with stacking schemes based on magnetic devices. This gives useful indications, although our selected stacking schemes are not optimized. Indeed, the magnetic recombination is obtained by emittance juxtaposition in the phase space either along x or along the x' axis of the two incoming beams, simply assuming a final separation of 6σ of the recombined beam centroids. Figure 5 illustrates the phase space obtained by stacking Beam1 and Beam2 along x' (5a) or along x (5b), with axis separations $\delta x' = 3 \times \theta_c = 48$ μrad and $\delta x = 6 \times \sigma_x = 1.2$ mm, respectively. A two-dimensional Gaussian fit is performed to obtain contour lines in the phase space that contains 68% and 95% of the total population, respectively. In the case of crystal assisted merging, the fit in the x' direction was performed considering the convolution of three Gaussian peaks of interest i.e., the CH beam and the two obtained selecting the VR-AM region. The parameters of the superimposed distributions are reported in Table 3, where the RMS emittance ϵ_{RMS} is evaluated as the product $\sigma_x \times \sigma_{x'}$ [19]. The higher ϵ_{RMS} for crystal assisted merging is in our opinion due to the MCS occurring because of the particle interactions with a 4 mm crystal and to dechanneled particles of Beam1 emerging from the crystal in a direction too close to the CH one. To mitigate the latter issue, we believe that a larger bending angle should help in producing a more suitable density distribution to allow scraping of the dechanneled particles. It is worth observing that the crystal merging produces an occupancy of the phase space where it should be easy to scrape the unwanted particles surrounding the core, while transverse stacking distribution is depleted around the phase-space center.

Fig. 4 Phase-space distribution density of the merged beam at the crystal exit face. The level contours highlight the 68% and the 95% fractions of the merged population (black dashed). Histogram projections on x and x' axes show the superposition of all the particle tracks (black) and the 2D Gaussian fit (green hue) for the evaluation of ϵ_{RMS} in Table 3

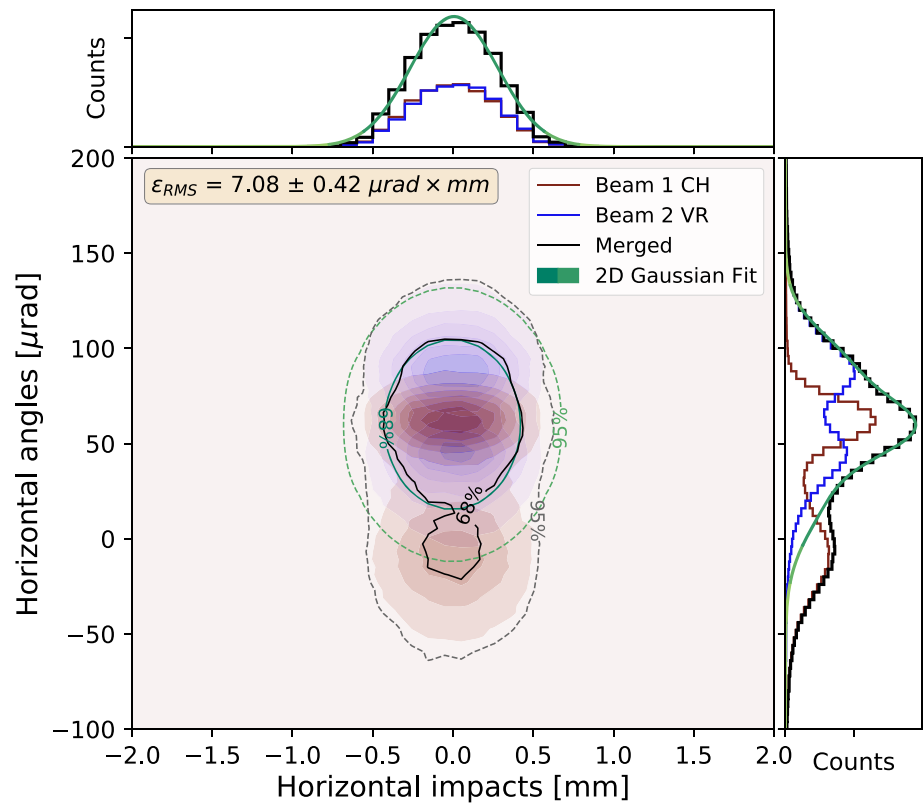


Fig. 5 Stacking distribution in the phase space (x, x'). The two beams are colored in red and blue hue. The best fit of the combined population is shown by the contour lines (green hue) at 68% and 95% of the total number of particles. The populations are fitted to two-dimensional Gaussian function

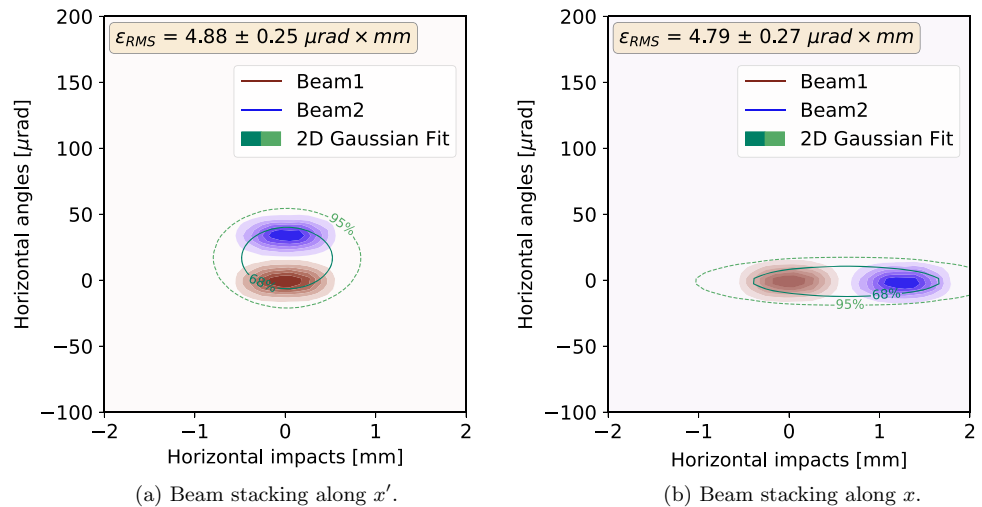


Table 3 Merging performance: μ and σ are the two-dimensional Gaussian mean values and standard deviations in the respective direction of the phase space; ϵ_{RMS} is the RMS emittance

	μ_x mm	$\mu_{x'}$ μrad	σ_x mm	$\sigma_{x'}$ μrad	ϵ_{RMS} mm μrad
Stacking along x'	0.02 ± 0.01	17.2 ± 0.5	0.32 ± 0.01	15.1 ± 0.5	4.88 ± 0.25
Stacking along x	0.62 ± 0.03	-0.15 ± 0.28	0.66 ± 0.03	7.25 ± 0.28	4.79 ± 0.27
Crystal merging	-0.01 ± 0.01	61.5 ± 1.1	0.26 ± 0.01	27.0 ± 1.1	7.08 ± 0.42

5 Conclusions

In this paper, a possible scheme to merge beams using bent crystals has been discussed. A first estimate of the performance of the crystal assisted beam merging has been successfully carried out, by reprocessing data collected by the UA9 Collaboration. Two-beam merging in a bent crystal and transverse stacking with magnets have similar performance, although the latter is rather schematic. The novel merging method extends the potential applications of bent crystals in accelerators. Compared to conventional techniques,

the method under discussion requires compact and inexpensive installations, possibly of interest for future muon colliders. The demonstration of principle obtained by reprocessing experimental data is fast and in our opinion very robust, for which the shortness of the injection chain is of paramount importance. Our conclusion substantiates the importance of an experimental test of beam merging assisted by a bent crystal at the upgraded UA9 installation in the CERN North Area to be carried out as soon as possible. Optimization of the beam merging process will be performed by varying the direction and the emittance of the incoming beams and the crystal parameters. Simulations based on Geant4 and FLUKA have begun to extend and accelerate detailed comprehension of the merging process, including for low-energy beams.

Acknowledgements We would like to gratefully acknowledge the activity of the past members of the UA9 Collaboration who contributed to acquire the data and the Russian colleagues from PNPI Gatchina who built and provided to the Collaboration the crystal ACP80. Imperial College gratefully acknowledges financial support from the UK Science and Technology Facilities Council.

Data availability This manuscript has no associated data. [Authors' comment: All the relevant data from measurements at the SPS North Area are reported in the paper and the analysis used to produce the results is described.]

Open Access This article is licensed under a Creative Commons Attribution 4.0 International License, which permits use, sharing, adaptation, distribution and reproduction in any medium or format, as long as you give appropriate credit to the original author(s) and the source, provide a link to the Creative Commons licence, and indicate if changes were made. The images or other third party material in this article are included in the article's Creative Commons licence, unless indicated otherwise in a credit line to the material. If material is not included in the article's Creative Commons licence and your intended use is not permitted by statutory regulation or exceeds the permitted use, you will need to obtain permission directly from the copyright holder. To view a copy of this licence, visit <http://creativecommons.org/licenses/by/4.0/>.

References

1. J. Lindhard, et al., *Influence of crystal lattice on motion of energetic charged particles*, Munksgaard Copenhagen, **34** (1965)
2. E.N. Tsyganov, Fermilab Preprint TM-682. Fermilab, Batavia. FERMILAB-TM-0682 (1976)
3. A. Taratin, Phys. Part. Nucl. **29**(5), 437 (1998)
4. W. Scandale, A. Taratin, Phys. Rep. **815**, 1 (2019)
5. A. Taratin, S. Vorobiev, Phys. Lett. A **119**(8), 425 (1987)
6. N. Doble, L. Gatignon, P. Grafström, Nucl. Instrum. Methods Phys. Res., Sect. B **119**(1–2), 181 (1996)
7. V. Fanti, A. Lai, D. Marras, L. Musa, A. Nappi, R. Batley, A. Bevan, R. Dosanjh, R. Galik, T. Gershon et al., Nucl. Instrum. Methods Phys. Res., Sect. A **574**(3), 433 (2007)
8. A. Afonin, V. Baranov, V. Biryukov, M. Breese, V. Chepegin, Y.A. Chesnokov, V. Guidi, Y.M. Ivanov, V. Kotov, G. Martinelli et al., Phys. Rev. Lett. **87**(9), 094802 (2001)
9. A. Afonin, V. Baranov, V. Biryukov, V. Chepegin, Y. Fedotov, V. Kotov, V. Maishev, V. Terekhov, E. Troyanov, et al., arXiv preprint hep-ex/0207040 (2002)
10. F. Velotti, P. Bestmann, M. Butcher, M. Calviani, M. Di Castro, M. Donze, L. Esposito, M. Fraser, S. Gilardoni, B. Goddard, et al., in *10th Int. Particle Accelerator Conf. (IPAC'19), Melbourne, Australia, 19-24 May 2019* (JACOW Publishing, Geneva, Switzerland, 2019), p. 3399–3403
11. W. Scandale, G. Arduini, R. Assmann, C. Bracco, M. Butcher, F. Cerutti, M. D'andrea, L. Esposito, M. Garattini, S. Gilardoni et al., Int. J. Mod. Phys. A **37**(13), 2230004 (2022)
12. W. Scandale, F. Cerutti, L. Esposito, M. Garattini, S. Gilardoni, A. Natchii, R. Rossi, G. Smirnov, V. Zhovkovska, F. Galluccio et al., Eur. Phys. J. C **80**, 1 (2020)
13. F. Cole, M. Tigner, Particle accelerators. Tech. rep., Fermi National Accelerator Lab. (FNAL), Batavia, IL (United States) (1985)
14. W. Scandale, A. Vomiero, E. Bagli, S. Baricordi, P. Dalpiaz, M. Fiorini, V. Guidi, A. Mazzolari, D. Vincenzi, R. Milan et al., Phys. Lett. B **681**(3), 233 (2009)
15. M. Pesaresi, W. Ferguson, J. Fulcher, G. Hall, M. Raymond, M. Ryan, O. Zorba, J. Inst. **6**(04), P04006 (2011)
16. G. Hall, G. Auzinger, J. Borg, T. James, M. Pesaresi, M. Raymond, Nucl. Instrum. Methods Phys. Res., Sect. A **924**, 394 (2019)
17. G. Hall, T. James, M. Pesaresi, J. Inst. **15**(05), C05014 (2020)
18. R. Rossi, L.S. Esposito, M. Pesaresi, G. Hall, W. Scandale, Track Reconstruction and Analysis of Particle Interactions in Short Bent Crystals (2023). Unpublished
19. A.W. Chao, K.H. Mess, M. Tigner, F. Zimmermann, *Handbook of Accelerator Physics and Engineering* (World scientific, New Jersey, 2013)